Available online at www.sciencedirect.com
SCIENCE DIRECT
Journal of Power Sources 147 (2005) 220–226
JOURNAL OF POWER SOURCES
www.elsevier.com/locate/jpowsour

New investigation of fluorine-substituted spinel $LiMn_2O_{4-x}F_x$ by using sol–gel process

J.T. Son *, H.G. Kim

Department of Materials Science and Engineering, Korea Advanced Institute of Science and Technology, 373-1 Kusong-dong, Yusong-gu, Taejon, South Korea

Received 30 August 2004; accepted 10 December 2004

Abstract

To investigate the electrochemical properties of $LiMn_2O_{4-x}F_x$ ($0 < x < 1$) as a cathode material for 4-V class lithium secondary batteries, spinel phases synthesized at 800 °C are examined. Although the initial discharge capacity of $LiMn_2O_4$ is improved by substitution of F^- for O^{2-} in the single-phase region, the cycle performance is reduced considerably compared with that of parent $LiMn_2O_4$. X-ray diffraction (XRD) data show that the single-phase region of x in $LiMn_2O_{4-x}F_x$ is $0 < x < 0.2$. A secondary phase (Mn_2O_3) is observed in the region $0.4 < x < 1.0$. Voltammetric peaks between 3 and 4.5 V region and XRD data suggest that the oxidation state of Mn in the parent $LiMn_2O_4$ increases at the expense of creating second phase (Mn_2O_3). These results also imply that a second phase spinel can improve the cycling performance of $LiMn_2O_4$ by suppressing the Jahn–Teller instability. The oxidation state of Mn in the single-phase spinel and the second-phase coexisting spinel is compared by means of XPS measurements. The electronic conductivity and activation energy of $LiMn_2O_4$ is also discussed.

Keywords: $LiMn_2O_4$; Fluorine; Electronic conductivity; Cycleabilty; Lithium secondary battery; Electrochemical properties

1. Introduction

The enormous growth in portable electronic devices, such as mobile phones and note-book computers, has led to an increasing demand for high energy and high power batteries [1,2]. Lithium secondary batteries have satisfied this demand to a greater degree than other battery systems [3,4].

In recent years, the normal spinel $LiMn_2O_4$ has been studied extensively as a cathode material for rechargeable lithium cells [5,6]. Its rechargeable capacity is equal to 100–130 mAh g^{-1} and is comparable with the capacity of the $LiCoO_2$ system [7]. In addition, $LiMn_2O_4$ is cheaper than $LiCoO_2$ or $LiNiO_2$ and more environmentally benign [8].

The discharge curve of $Li_xMn_2O_4$ exhibits two voltage plateaux, namely, 4 V for $0 < x < 1$ and 3 V for $1 < x < 2$. In the 3 V range, a severe loss of capacity with cycling is caused by a large volumetric change due to a structure phase transition from cubic to tetragonal, which is derived from the Jahn–Teller distortion of $Mn^{3+}(3d^4)$ [9]. Accordingly, the material can be cycled only in the 4 V range, albeit with marked capacity fading.

To improve the cycle performance in the 4 V range, many research groups have investigated the properties of manganese-substituted spinels $LiM_xMn_{2-x}O_4$ (M = Al, Cr, Ga, Ti, Ge, Fe, Co, Zn, Ni, Mg) [10–16]. These studies have shown that substitution of low valence-state metal cation for Mn enhances the stability of the spinel. Whereas, the cycle performance of the $LiM_xMn_{2-x}O_4$ is improved by substitution of M for Mn^{3+} in the octahedral sites, the discharge capacity is reduced considerably compared with that of the parent $LiMn_2O_4$.

A few researchers have examined the properties of oxygen-substituted spinels $LiMn_2O_4$. Recently, Amatucci et al. [17,18] have shown that the introduction of anion substitution can reduce the Mn oxidation state and improve the

* Corresponding author. Present address: MS 70-108B Advanced Energy Technology Division, LBNL, CA 94720, USA Tel.: +1 510 486 7140; fax: +1 510 486 7303.
E-mail address: jtson@lbl.gov (J.T. Son).

0378-7753/$ – see front matter © 2005 Elsevier B.V. All rights reserved.
doi:10.1016/j.jpowsour.2004.12.006

chemical stability of the spinel. Nevertheless, no explanation was given for the change in electrochemical properties displayed by oxygen-substituted spinels $LiMn_2O_4$. In addition, the authors [17,18] were opposed to the well known concept that a high Mn oxidation state enhances the stability of spinel and depresses the Jahn–Teller distortion of Mn^{3+} ($3d^4$) [10–16].

The aim of the present paper is to obtain more information on the electrochemical properties related to oxygen-substituted spinels $LiMn_2O_4$. These studies also aim to solve the controversy about the influence of the Mn oxidation state at the oxygen substituted spinel.

2. Experimental

2.1. Powder preparation

The sol–gel process was adapted to the synthesis of $LiMn_2O_{4-x}F_x$. In order to determine the doping effect of anions (O) on the structural and electrochemical properties, anions were substituted with F. A stoichiometric amount of Li and Mn acetate (Junsei Chemicals; 99%) salts with MnF (Junsei Chemicals; 99%) were dissolved in distilled water and mixed well with an aqueous solution of glycine (Aldrich, high purity). The glycine was used as a chelating agent to produce a gel, and the molar ratio of glycine to total metal ions was fixed at unity. Ammonium hydroxide was added slowly to this solution with constant stirring until pH 6 was achieved. The resultant solution was evaporated at 80 °C for 4 h until a transparent sol was obtained. To remove water, the sol was heated at 80 °C for 3 h. As the evaporation of water proceeded, the sol turned into a viscous transparent gel. The resulting gel precursors were calcined at 800 °C for 8 h in air to obtain the spinel phase.

Phase analysis was carried out by means of powder X-ray diffraction (XRD) with Cu Kα radiation in a Rigaku X-ray diffractometer. Scanning electron micrographs were obtained to examine the morphology of the powder. The average valence of manganese in the lithium manganese oxides was determined by using XPS.

2.2. Electrochemical measurements

A cathode electrode was prepared by mixing $LiMn_2O_4F$ powder with 10 wt.% carbon black (Vulcan, XC-72) and 5 wt.%PVDF (poly-vinylidene fluoride) in NMP (n-methyl pyrrodinone) solution. The stirred mixture was spread on a 316 stainless steel ex-met. The electrode specimens were dried under vacuum at 120 °C.

A three-electrode cell was constructed for charge–discharge experiments. An excess amount of lithium foil (Foote Mineral, 99.9%) was used as the negative electrode. The electrolyte was a 1 M $LiClO_4$–PC solution that was pre-mixed at Mitsubishi Chemicals (PC propylene carbonate). Galvanostatic charge–discharge experiments were performed with a potentiostat/galvanostat (EG&G PARC Model 263). The cut-off voltages were set at 4.5 and 3.0 V for charge and discharge, respectively, at a current density of 1 mA cm^{-2}(i.e., a rate of 0.5C).

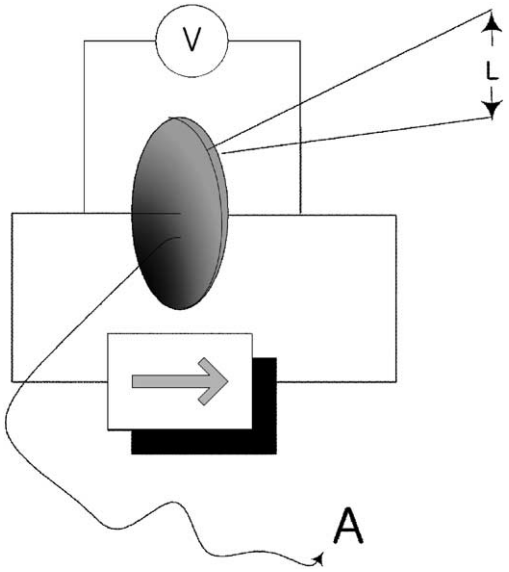

Fig. 1. Schematic diagram of the cell used for 2-probe measurements.

2.3. Electric conductivity measurements

The calcined powders were mixed with 5 wt.% PVDF and ball-milled in ethanol for 24 h. The resultant mixtures were then dried and pressed into pellets (1.2 cm in diameter) under a pressure of 100 MPa and re-fired at 800 °C for 8 h. The thickness of the tested samples varied from 0.80 to 1.01 mm. A minimum thickness was required to minimize the time for electrochemical equilibrium of the sample. The cell for 2-probe measurements consistsed of two silver films and one $LiM_xMn_{2-x}O_4$ pellet, as shown schematically in Fig. 1. Two silver wires were positioned to sense the resistance of the pellet.

3. Results and discussion

3.1. Structure characterization of $LiMn_2O_{4-x}F_x$

Transport gels could be formed for all the samples under investigation, and were transparent and uniform in colour. These features indicated the formation of homogeneous phases [19–21]. It is thought [19–21] that the carboxylic and amino groups on the glycine can form chemical bonds with the metal ions and that these mixtures develop extremely viscous polymeric resins as they become gels.

The XRD patterns for the $LiM_xMn_{2-x}O_4$ ($0 \leq x \leq 1$) powders are presented in Fig. 2. When the content of substituted F is small, $x \leq 0.2$, the samples are identified as a single phase with the space group *Fd*3*m* in which the lithium ions occupy

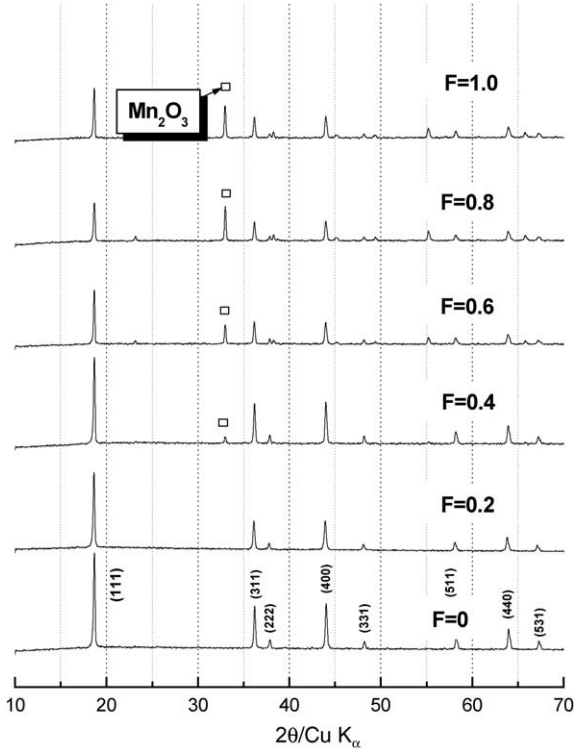

Fig. 2. X-ray diffraction patterns for $LiMn_2O_4F$ powders with F-contents.

the tetrahedral (8a) sites and the transition metal ions occupy the tetrahedral (16d) sites [19,22]. The observed diffraction lines match completely those of a cubic spinel $LiMn_2O_4$ structure listed in a JCPDS file. The sharp (4 0 0) peak of the un-doped sample reveals that highly crystallized manganese oxides have been synthesized [20]. The intensity of the (4 0 0) peak for $LiMn_2O_{3.8}F_{0.2}$ is less than that of $LiMn_2O_4$ [23]. This result reveals that F-doped samples have low crystalline structure and an unstable spinel framework. It is expected that this low crystalline structure will effect cycle-life. When the substituted F content is large, $0.4 \leq x \leq 1.0$, a new peak that belong to Mn_2O_3 is observed at $2\theta = 37.1$, see Fig. 2. The intensity of the Mn_2O_3 peak increases with increasing F content. Xiaomei et al. [9] claimed that this secondary phase is Li_2MnO_3. In our opinion, however, they could not discern this phase precisely due to the very small amont of F doping ($x = 0.045$). We carefully matched this second phase by using the JCPDS file and also calculated the lattice parameters by using X-ray analysis tools; the results are given in Table 1.

Table 1
Dependence of lattice parameter for $LiMn_2O_4$ and Mn_2O_3 the F substituted composition

$LiMn_2O_{4-x}O_4$	a (Å) of $LiMn_2O_4$	a (Å) of Mn_2O_3	Mn_2O_3 phase
$x = 0$	8.224 ± 0.001		×
$x = 0.2$	8.2408 ± 0.0007		×
$x = 0.4$	8.2277 ± 0.001	9.4002 ± 0.0007	◯
$x = 0.6$	8.2288 ± 0.0004	9.4004 ± 0.0007	◯
$x = 0.8$	8.2285 ± 0.0006	9.401 ± 0.001	◯
$x = 1.0$	8.2269 ± 0.0007	9.408 ± 0.001	◯

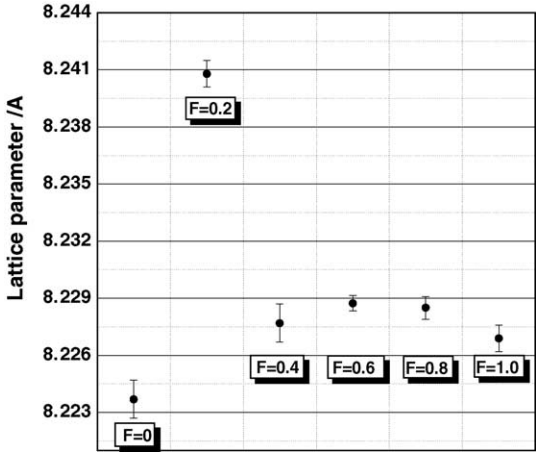

Fig. 3. Effect of F-content on lattice parameter of $LiMn_2O_4$.

The value of the average oxidation state of manganese in the spinel phase is related closely to the lattice constant of the cubic unit cell [24,25]. For example, MnO_2 (all Mn^{4+}) transforms progressively to MnO_2 (all Mn^{3+}) for the binary Mn oxide system as the temperature is increased [19]. The atomic radius of Mn^{3+} (0.72 Å) is larger than that of Mn^{4+} (0.67 Å) and thus the lattice constant of the cubic unit cell of the spinel $LiMn_2O_4$ powders with low oxidation states of Mn is larger than that of powders with corresponding high oxidation states.

The effect of F substitution on the lattice constant is demonstrated in Fig. 3. The lattice constant increases almost up to 8.240 Å when the substituted F contents is increased from 0 to 0.2 in the solid solution range. This trend is opposite to what is expected by Vegard's rule for the substitution of O for the smaller F anion. Therefore, the increase in lattice parameter can be assumed to originate from an increase in the quantity of the larger trivalent manganese Mn^{3+}. The lattice constant decreases down to about 8.230 Å when the amount of substituted F is large, $0.4 \leq x \leq 1.0$. These results suggested that the Mn oxidation state of the parent $LiMn_2O_4$ increased at the expense of creating a second phase (Mn_2O_3). Therefore, the data imply that a second phase (Mn_2O_3) of coexisting spinel can enhance the cycling performance above that of than $LiMn_2O_4$ by suppressing the Jahn–Teller instability. On the other hand, the capacity will decrease almost linearly due to development of a second phase (Mn_2O_3) that is known to be an inactive battery material.

The effect of F substitution on the lattice constant of Mn_2O_3 is shown in Fig. 4. The lattice parameter of Mn_2O_3 becomes larger (up to 9.408 Å) with increasing F content.

Scanning electron micrographs of $LiMn_2O_4$ powders calcined at 800 °C for 8 h in air are presented in Fig. 5. As the F content is increased, the Mn_2O_3 content is increased and the shape of the powder transforms into a facet form of larger crystal size, i.e., the size grows from 50 to 200 nm. These observations imply that the Mn_2O_3 phase accelerates the growth kinetics.

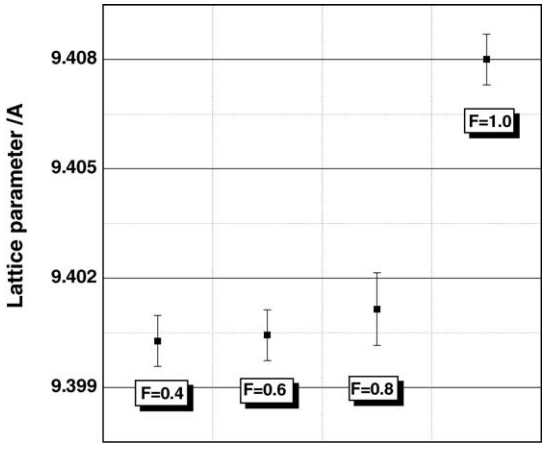

Fig. 4. Effect of F-content on lattice parameter of Mn_2O_3.

X-ray photoelectron spectroscopy (XPS) studies were undertaken to elucidate the change in the chemical state of the synthesized $LiMn_2O_4$. The results are given in Fig. 6. The Mn ($2p_{3/2}$) emission shifts from 641.6 to 642.9 eV when the F content is increased from 0 to 1.0. This means that the average oxidation state tends to decrease at high F content. The binding energy for Mn standards and previously reported XPS reference data [26] are compared in Fig. 7.

From the above findings, it is concluded that $LiMn_2O_4$ powders with wide differences in material properties, such as crystallity, Mn oxidation state, and particle size, and shape can be produced in a controlled manner by varying the substituted F content.

3.2. Electrochemical characterization

The initial charge curves of Li|$LiMn_2O_4$ cells at a constant charge–discharge rate of *C*/2 over a voltage range of 4.5 to 3.0 V are given in Fig. 8. The theoretical and experimental capacities are compared in Table 2. The theoretical capacity is 148 mAh g^{-1} on the basis that one Li per Mn_2O_4 unit is reversibly intercalated and deintercalated at 4.1 V. In practice, $LiMn_2O_4$ shows about 123 mAh g^{-1} which corresponds to only 0.83 of the total Li in $LiMn_2O_4$ being utilized within the selected voltage range. The Li|$LiMn_2O_{3.8}F_{0.2}$ cell exhibited a capacity of 132 mAh g^{-1}, the increase in the capacity is due to the reduction of some Mn^{4+} to Mn^{3+} during fluorine substitution. The use of monovalent fluorine substitution for divalent oxygen increases the amount of Mn^{3+} content available for the redox process (therefore increasing the specific capacity). When the substituted F content is large, i.e., $0.4 \leq x \leq 1.0$, the initial capacity is decreased dramatically because of the increase in the amount of the new phase (Mn_2O_3). The Mn_2O_3 phase is believed to not participate in Li intercalation and de-intercalation at a constant charge–discharge rate of *C*/2 over the voltage range of 4.5 to 3.0 V.

Table 2
Initial discharge capacity of substituted $LiMn_2O_4$

Spinels $LiMn_2O_{4-x}F_x$	Capacity reduction (%)	Discharge capacity (mAh g^{-1})	
		Predicted	Experimental
$x = 0$	17	148 (theoretical)	123.01
$x = 0.2$	10	147.5	132.13
$x = 0.4$	22	147	113.96
$x = 0.6$	60	146.5	58.68
$x = 0.8$	65	145.9	51.39
$x = 1.0$	60	144.6	57.63

Cyclic voltammograms for $LiMn_2O_4$ and substituted spinel are presented in Fig. 9. There are two anodic and cathodic peaks for $LiMn_2O_4$ and the substituted spinel. The two pairs of oxidation and reduction peaks for the spinel are located around 4.15 and 4.0 V, and correspond to two-

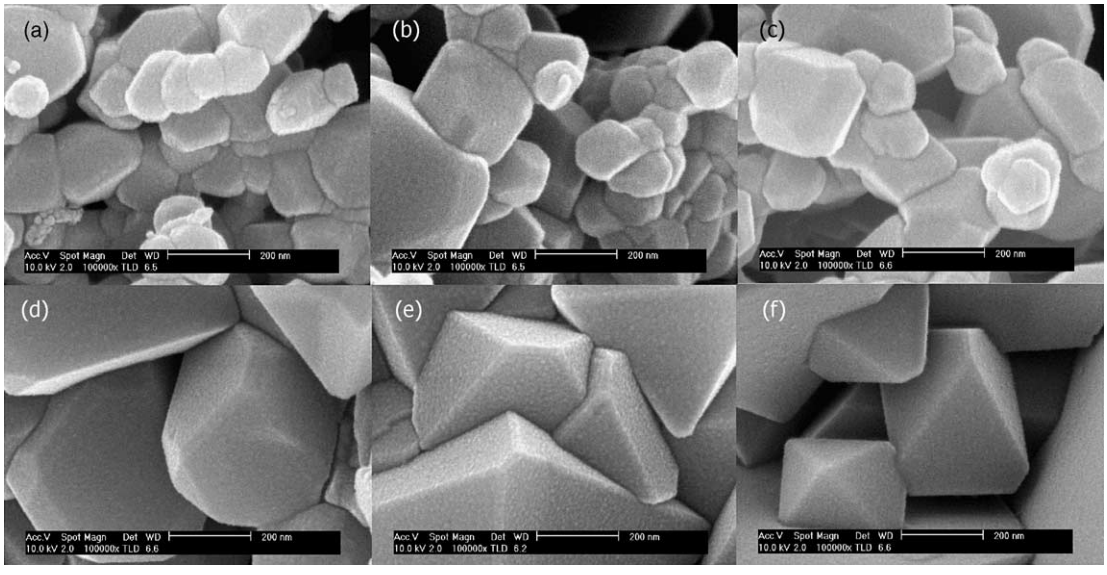

Fig. 5. Scanning electron micrographs of $LiMn_2O_4$ powders as function of F content: (a) F = 0 (b) F = 0.2 (c) F = 0.4 (d) F = 0.6 (e) F = 0.8 (f) F = 1.0.

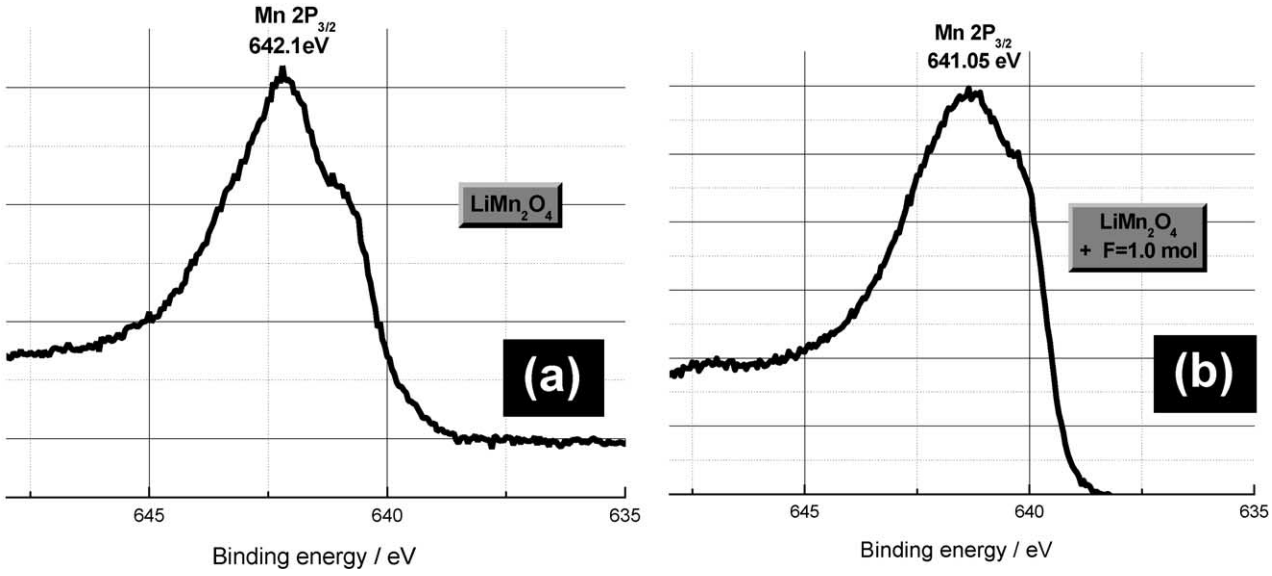

Fig. 6. XPS emission Mn (2P) of $LiMn_2O_4$ powders: (a) F = 0 (b) F = 1.0.

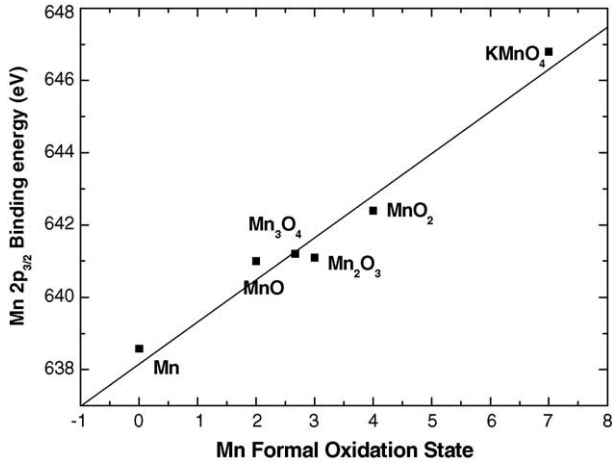

Fig. 7. X-ray photoelectron spectra of binding energy for Mn standards and relative to literature reference materials [26].

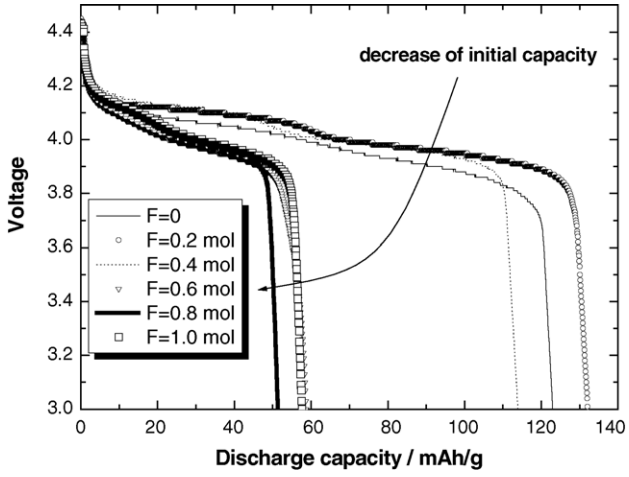

Fig. 8. Initial discharge behaviour of $LiMn_2O_4$ as function of F content.

stage reversible intercalation/de-intercalation processes of lithium. The following are new observations in this investigation. The 4.15-V peak current densities as well as area under the current–voltage curve for the F-substituted spinels are, respectively, lower and smaller than those for the 4.10-V peak and $LiMn_2O_4$. Because the oxidation of Mn^{3+} to Mn^{4+} occurs only in the 4.15 V range, it is reasonable to assume that only Mn^{3+} in the F-substituted spinel gives rise to the oxidation-reduction peaks and that the amount of Mn^{3+} is decreased by F-doping and, thereby, results in a decrease in the observed peak current and area. Note, the decrease in Mn^{3+} by F doping has also been discussed above in Section 3.1.

The cyclic voltammetric behaviour is very similar to that of cation doping [27], but the mechanism of Mn^{3+} to Mn^{4+} is quite different, i.e.,

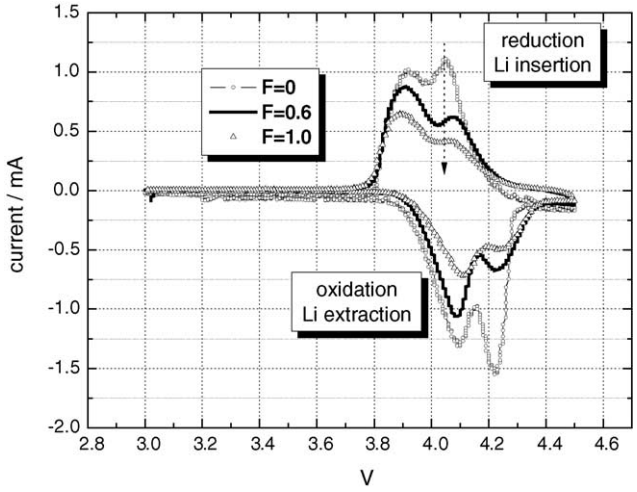

Fig. 9. Cyclic voltamograms for $LiMn_2O_4$ and substituted $LiMn_2O_4$ at sweep rate of 0.1 mV s^{-1}.

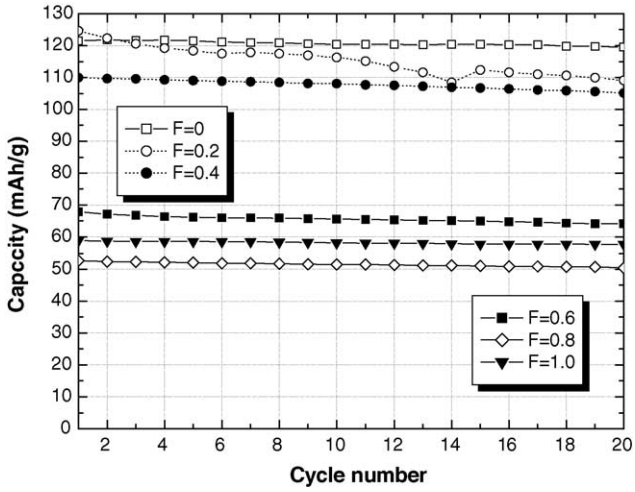

Fig. 10. Discharge capacity of Li|$LiMn_2O_4$ cell as function of F content.

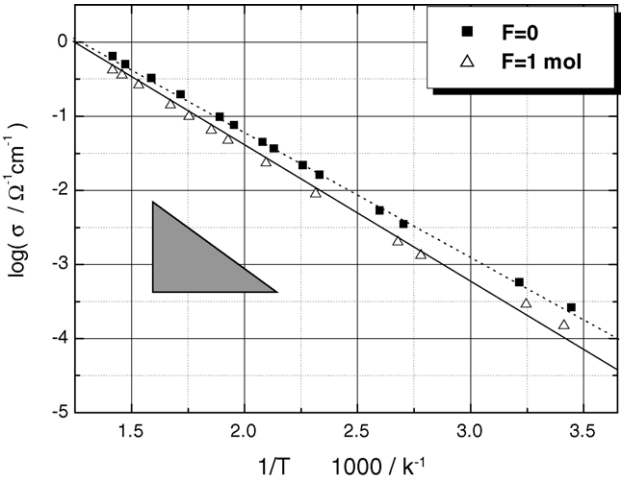

Fig. 11. Temperature dependence of electronic conductivities.

(i) *Cation substitution for Mn*: oxidation state of Mn in parent $LiMn_2O_4$ increases to maintain charge-neutrality condition.
(ii) *F-substitution for O*: oxidation state of Mn in parent $LiMn_2O_4$ increases at the expense of creating a second phase (Mn_2O_3).

Plots of discharge capacity with cycling are shown Fig. 10. The discharge capacity of pure $LiMn_2O_4$ decreases slowly during cycling, and after 20 cycles about 98% of the initial capacity can be recovered. By contrast, capacity fading during cycling is faster with a Li|$LiMn_2O_{3.8}F_{0.2}$ cell. The capacity loss is 13% of the initial value after 20 cycles. Based on simple electroneutrality concepts, applying a mono-valence F-substitution to a spinel phase would lead to a lowering of the Mn oxidation state, which is the opposite of what is electrochemically desirable for long cycle-life.

When the substituted F content is large, $0.4 \leq x \leq 1.0$, the capacity fading during cycling is decreased. This can be explained by postulating that Mn oxidation state in the parent $LiMn_2O_4$ increases at the expense of creating a second phase (Mn_2O_3). Therefore, it is electrochemically desirable for long cycle-life.

To evaluate the influence of F substitution on the electronic properties, two types of sample were investigated, namely:

sample A: $LiMn_2O_4$ (fluorine substitution: 0 mol).
sample B: $LiMn_2O_{4-x}F_x + Mn_2O_3$ (fluorine substitution: 1 mol).

The temperature dependence of the electrical conductivity of the $LiMn_2O_4$ spinel obtained in the temperature range 300 to 700 K in an air atmosphere is given in Fig. 11. Since electronic conduction in the $LiMn_2O_4$ spinel is believed to be due to electrons hopping between mixed valences of Mn [28], the dependence of the electrical conductivity of $LiMn_2O$ on temperature is given by:

$$\sigma = \frac{\sigma_0}{T} N_v x(1-x) \exp\left(\frac{-E_h}{kT}\right) \quad (1)$$

where: σ is the electrical conductivity; T is the absolute temperature; k is the Boltzmann constant; e is the electron charge; E_h is the activation energy for hopping; N_v is the effective density of states in the valence band; and x is the portion of lattice occupied with mobile species.

The electrical conductivity of pure $LiMn_2O_4$ is higher than that of a F-substituted sample at room temperature. The lower conductivity of the latter can be explained by a decrease in the density of Mn^{4+} states available for the electrons with Mn^{3+}. Molenda et al. [29] also observed a decrease in conductivity with increasing Mn^{3+}.

There are some discrepancies in the literature with respect to the electrical properties of $LiMn_2O_4$. For example, Pistoia et al. [30] indicated that $LiMn_2O_4$ was a hopping semiconductor with conductivity of about $2 \times 10^{-6}\,\Omega^{-1}\,cm^{-1}$, while Chen et al. [31] reported that the total conductivity was closed to $10^{-4}\,\Omega^{-1}\,cm^{-1}$ at room temperature, as determined from impedance measurement. Feltz et al. [32] found that the electronic conductivity of $LiMn_2O_4$ was about $2.3 \times 10^{-4}\,\Omega^{-1}\,cm^{-1}$ at room temperature from d.c. measurements. In the study reported here, the electronic conductivity of $LiMn_2O_4$ is $5 \times 10^{-4}\,\Omega^{-1}\,cm^{-1}$ at room temperature from a 2-probe d.c. measurements while that for F-substituted (1 mol) was $LiMn_2O_4$ is $2 \times 10^{-4}\,\Omega^{-1}\,cm^{-1}$.

The activation energies obtained for a particular series of $LiMn_2O_4$ samples as a function of lattice parameter is given in Fig. 12. The activation energy increases with increasing value of the lattice parameter. According to the proposed theory [29], this might indicate that activation energy is connected with charge transport through cationic states Mn^{3+} and Mn^{4+}. The small lattice size implies more overlap in the wave functions of neighbouring Mn ions with different valence states, which thus leads to a low electrical activation energy. In this investigation, the electronic activation energy

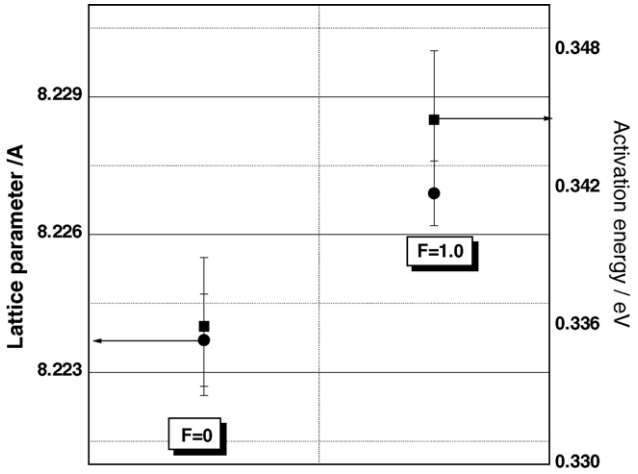

Fig. 12. Relationship between electrical activation energy and lattice parameter.

of $LiMn_2O_4$ and F-substituted (1 mol) $LiMn_2O_4$ is 0.336 and 0.345, respectively. Similar values have been reported by Molenda et al. [29] for low-temperature calcined material.

4. Conclusions

Fluorine-substituted spinel $LiMn_2O_{4-x}F_x$ powders with sub-micron, mono dispersed, and highly homogeneous particles have been synthesized by a sol–gel method using an aqueous solution of metal acetate that contains glycine as a chelating agent. The following observations are made.

(i) Compared with a $Li|LiMn_2O_4$, the $Li|LiMn_2O_{3.8}F_{0.2}$ cell exhibits a high capacity of 132 mAh g^{-1}. This is due to the reduction of some Mn^{4+} to Mn^{3+} during F-substitution. Monovalent fluorine substitution for divalent oxygen increases the amount of Mn^{3+} content available for redox reactions.

(ii) The discharge capacity of pure $LiMn_2O_4$ decreases slowly during cycling, and after 20 cycles about 98% of the initial capacity can be recovered. By contrast, capacity fading during cycling is faster for a $Li|LiMn_2O_{3.8}F_{0.2}$ cell. The capacity loss is 13% of the initial value after 20 cycles. This behaviour can be explained by postulating that a F-substituted spinel phase will lead to a lowering of the Mn oxidation state, the opposite of what is electrochemically desirable for long cycle life.

(iii) The electronic conductivity of $LiMn_2O_4$ synthesized by a sol–gel method is $5 \times 10^{-4}\,\Omega^{-1}\,cm^{-1}$ at room temperature from 2-probe d.c. measurements, and $2 \times 10^{-4}\,\Omega^{-1}\,cm^{-1}$ for the F-substituted (1 mol) counterpart.

(iv) The electronic activation energy of $LiMn_2O_4$ is 0.336 and 0.345 for $LiMn_2O_4$ and F-substituted (1 mol) $LiMn_2O_4$, respectively. An increase in activation energy is observed with increasing value of lattice parameter. This behaviour can be explained by postulating that the small lattice size implies more overlap in the wave functions of neighbouring Mn ions with different valence states, which gives a low electrical activation energy.

References

[1] J.R. Dahn, U.V. Scken, C.A. Michal, Solid State Ionics 44 (1990) 87.
[2] D. Guyomard, J.M. Tarascon, Solid State Ionics 69 (1994) 222.
[3] M.M. Thackeray, P.J. Johnson, L.A. de Piccioto, P.G. Bruce, J.B. Goodenough, Mater. Res. Bull. 19 (1984) 179.
[4] T. Ohuzuka, M. Kitagawa, T. Hirani, J. Electrochem. Soc. 137 (1990) 769.
[5] J.T. Son, K.S. Park, H.G. Kim, H.T. Chung, J. Power Sources 126 (2004) 182.
[6] J.T. Son, K.S. Park, H.G. Kim, H.T. Chung, J. Mater. Sci. 39 (2004) 3635.
[7] T. Ohuzuka, A. Ueda, M. Nagayama, J. Electrochem. Soc. 140 (1993) 1862.
[8] J.M. Tarascon, E. Wang, F.K. Shokoohi, W.R. Mckinnon, S. Colson, J. Electrochem. Soc. 138 (1991) 2859.
[9] W. Xiaomei, Z. Xiangfu, Y. Qinghe, J. Zhongkao, W. Haoqing, J. Fluorine Chem. 107 (2001) 39.
[10] R. Bittihn, R. Herr, D. Doge, J. Power Sources 43 (1993) 233.
[11] L. Guohua, H. Ikuta, T. Uchida, M. Wakihara, J. Electrochem. Soc. 143 (1996) 178.
[12] R.J. Gummow, A. de Kock, M.M. Thakeray, Solid State Ionics 69 (1994) 59.
[13] A.D. Robertson, S.H. Lu, W.F. Howard, J. Electrochem. Soc. 144 (1997) 3500.
[14] A.D. Robertson, S.H. Lu, W.F. Howard, J. Electrochem. Soc. 144 (1997) 3505.
[15] F. Le Cras, D. Bloch, M. Anne, P. Strobel, Solid State Ionics 203 (1996) 89.
[16] G. Pistoia, G. Wang, Solid State Ionics 66 (1993) 135.
[17] G.G. Amatucci, A.S. Gozdz, C. Schmutz, F.K. Shokoohi, J.M. Tarascon, Solid State Ionics 86 (1996) 49.
[18] G.G. Amatucci, A.S. Gozdz, C. Schmutz, F.K. Shokoohi, J.M. Tarascon, J. Power Sources 81 (1995) 39.
[19] Y.K. Sun, D.W. Kim, Y.M. Choi, J. Power Sources 79 (1999) 231.
[20] P.A. Lessing, Ceram. Bull. 66 (1989) 1002.
[21] M.S.G. Baythoun, F.R. Sale, J. Mater. Sci. 17 (1982) 2757.
[22] M.M. Thackeray, L.A. de Picciotto, A. de Kock, P.J. Johnson, V.A. Nocholas, K.T. Adendorff, J. Power Sources 21 (1986) 1.
[23] D.S. Ahn, M.Y. Song, J. Electrochem. Soc. 147 (2000) 874.
[24] T. Tsumura, M. Inagaki, Solid State Ionics 104 (1997) 36.
[25] C. Tsang, A. Manthiram, Solid State Ionics 89 (1996) 305.
[26] W.P. Kilroy, S. Dallek, J. Zaykoski, J. Power Sources 105 (2002) 75.
[27] H.J. Bang, V.S. Donepudi, J. Prakash, Electrochim. Acta 48 (2002) 443.
[28] J. Guan, M. Liu, Solid State Ionics 110 (1998) 21.
[29] J. Molenda, K. Swierczek, W. Kucza, J. Marzec, A. Stoklosa, Solid State Ionics 123 (1999) 155.
[30] G. Pistoia, D. Zane, Y. Zhang, J. Electrochem. Soc. 142 (1995) 2551.
[31] L. Chen, J. Schoonman, Solid State Ionics 67 (1994) 17.
[32] J. Topher, A. Feltz, J. Alloys Comp. 202 (1993) 231.